Research Article

Usman Afzal, Maddina Dinesh Kumar, Adnan Ashique, Nehad Ali Shah, and Jae Dong Chung*

Magnetohydrodynamics heat transfer rate under inclined buoyancy force for nano and dusty fluids: Response surface optimization for the thermal transport

https://doi.org/10.1515/ntrev-2025-0190
received December 14, 2024; accepted June 6, 2025

Abstract: The aim of this study is to analyze the heat transfer rate under inclined buoyancy force for nano and dusty fluids by incorporating key parameters such as the Prandtl number, volume fraction, fluid interaction parameter for temperature, and fluid-particle interaction parameter for velocity in the presence of magnetohydrodynamics (MHD) effects. The investigation focuses on understanding how these parameters influence velocity and heat transfer behavior in a porous medium. Nano and dusty fluids are crucial for thermal systems, environmental regulation, and materials processing. Unlike previous studies, this work examines their combined effects and employs response surface methodology (RSM) for optimization. The governing nonlinear ordinary differential equations are derived *via* similarity transformations and solved using bvp4c in MATLAB. RSM is employed to analyze parametric effects and determine optimal conditions for heat transfer enhancement. Higher Local Grashof number increases flow rate but decreases heat transfer rate. MHD and porosity effects significantly impact velocity and temperature. Dust-fluid interactions affect boundary layer behavior and heat transfer rates. Dusty fluid interactions influence boundary layer thickness and heat transfer. Findings are applicable in heat exchangers, electronics cooling, and industrial furnaces. The study offers a foundation for hybrid nanofluids, time-dependent flows, and fractional modeling in future research.

Keywords: inclined buoyancy force, dust particles, stretching sheet, volume fraction, magnetohydrodynamics, response surface optimization

*** Corresponding author: Jae Dong Chung,** Department of Mechanical Engineering, Sejong University, Seoul, 05006, Republic of Korea, e-mail: jdchung@sejong.ac.kr
Usman Afzal: Department of Mechanical Engineering, Sejong University, Seoul, 05006, Republic of Korea, e-mail: usmanafzal9884@gmail.com
Maddina Dinesh Kumar: Department of Mathematics, Saveetha School of Engineering, Saveetha Institute of Medical and Technical Sciences, Saveetha University, Chennai, 602105, Tamil Nadu, India, e-mail: dineshmaddina319@gmail.com
Adnan Ashique: Department of Mechanical Engineering, Sejong University, Seoul, 05006, Republic of Korea, e-mail: adnanashique1@gmail.com
Nehad Ali Shah: Department of Mechanical Engineering, Sejong University, Seoul, 05006, Republic of Korea, e-mail: nehadali199@yahoo.com

Nomenclature

B_0	induced magnetic field ($kg^2\ s^{-2}\ c^{-2}$)
Bi	Biot number
$(c_p)_{nf}$, c_m	specific heat of the nanofluids and dust particles ($m^2\ s^{-2}\ K^{-1}$)
Cf	skin friction
c	stretching sheet parameter (s^{-1})
Ec	Eckert number
k_{nf}	thermal conductivity ($kg\ m\ K^{-1}\ s^{-3}$)
f, F	dimensionless velocity of nanofluids and dust particles
Gr	local Grashof number
g	acceleration due to gravity ($m\ s^{-2}$)
K	Stokes resistance ($kg\ s^{-1}$)
K_1	porosity parameter
k_1	permeability of porous medium (m^2)
M	magnetic field parameter
m	mass of the dust particle (kg)
N	number density of the dust particles $\left(\frac{\text{particles}}{m^3}\right)$
Nu_x	Nusselt number
Pr	Prandtl number
Re_x	local Renolds number
T	nanoparticles temperature (K)
T_P	dust particles temperature (K)
T_w	temperature at surface (K)
T_∞	ambient temperature (K)
(u, v)	velocity components of nanofluids ($m\ s^{-1}$)

(u_p, v_p)	velocity components of dust phases (m s^{-1})
ν_{nf}	kinematic viscosity of nanofluids (m^2 s^{-1})
x, y	coordinates axes (m)
ϕ_P	volume fraction percentage of the dust particles
ρ_{nf}	density of the nanofluids (kg m^{-3})
σ	electrical conductivity (kg^{-1} m^{-3} s c^2)
μ	dynamic viscosity (kg m^1 s^{-1})
τ_T, τ_v	thermal equilibrium and relaxation time of dust particles (s)
θ, θ_p	dimensionless temperature
α	mass concentration of dust particles
β	fluid particle interaction parameter for velocity
β_T	fluid interaction parameter for temperature
γ	ratio of specific heat of nanoparticles to dust particles
ϕ_p	dust particles volume fraction

Homogeneity of dimensionless parameter:

$$\mathrm{Gr} = \frac{g\beta^*(T_w - T_\infty)}{cU_w} = \frac{\mathrm{m\,s^{-2}K^{-1}K}}{\mathrm{s^{-1}m\,s^{-1}}} = 1$$

$$M = \frac{\sigma B_0^2}{c\rho_{nf}} = \frac{(\mathrm{kg^{-1}\ m^{-3}\ c^2\ s})(\mathrm{kg^{-2}\ c^{-2}\ s^{-2}})}{\mathrm{s^{-1}\ kg\ m^{-3}}} = 1$$

$$\mathrm{Pr} = \frac{\mu_{nf}(c_p)_{nf}}{k_{nf}} = \frac{(\mathrm{kg\ m^{-1}\ s^{-1}})(\mathrm{m^2\ s^{-2}\ K^{-1}})}{\mathrm{kg\ m\ K^{-1}\ s^{-3}}} = 1$$

$$\alpha = \frac{\mathrm{Nm}}{\rho_{nf}} = \frac{\mathrm{m^{-3}\ kg}}{\mathrm{kg\ m^{-3}}} = 1$$

$$\beta = \frac{K}{c_m} = \frac{\mathrm{kg\ s^{-1}}}{\mathrm{s^{-1}\ kg}} = 1$$

$$K_1 = \frac{\nu_{nf}}{ck_1} = \frac{\mathrm{m^2\ s^{-1}}}{\mathrm{s^{-1}\ m^2}} = 1$$

$$\gamma = \frac{(c_p)_{nf}}{c_m} = \frac{\mathrm{m^2\ s^{-2}\ K^{-1}}}{\mathrm{m^2\ s^{-2}\ K^{-1}}} = 1$$

$$\mathrm{Ec} = \frac{cl^2}{A(c_p)_{nf}} = \frac{\mathrm{s^{-1}\ m^2}}{\mathrm{K\ m^2\ s^{-2}\ K^{-1}}} = 1$$

$$\beta_T = \frac{1}{c\tau_T} = \frac{1}{\mathrm{s^{-1}\ s}} = 1$$

1 Introduction

Fluids represent fundamental elements within both natural and engineered systems, recognized for their capacity to flow and adapt to the contours of their respective containers. They encompass both liquids and gases, distinguished by attributes such as viscosity and pressure. Varieties of fluids include ideal fluids (theoretical, devoid of viscosity), real fluids (exhibiting quantifiable viscosity), and Newtonian fluids, where the strain rate and shear stress are directly proportional, as exemplified by water and air. Non-Newtonian fluids, including blood and various polymers, display intricate behaviors characterized by stress-dependent viscosity [1]. In the field of engineering, fluids play a pivotal role in applications like hydraulic systems, turbines, and pumps, enabling power transmission, energy generation, and various industrial processes [2].

Applications for studying heat transfer and fluid flow over a stretching surface are significant in many engineering domains. Conventional fluids like oil, ethylene glycol, and water often exhibit low thermal conductivity, posing challenges in designing efficient electronic systems. To overcome this, researchers have enhanced base fluids through the integration of nanoparticles, resulting in nanofluids, or by adding micrometer-sized particles, leading to dusty fluids, both of which boost thermal conductivity. While previous studies have largely focused on nanofluids or dusty fluids separately, this investigation explores the combined momentum and thermal transfer properties of dusty nanofluids – a combination of conductive dust particles and nanoparticles. This innovative approach aims to further improve the thermal performance of base fluids for specific applications [3]. Certainly, the stability of laminar flow in fluids containing evenly spaced dust particles has been thoroughly analyzed. Subsequent studies have investigated magnetohydrodynamics (MHD) flow, examining heat and momentum exchange [4]. This work builds upon previous research by focusing on the impact of nanoparticle size on velocity, temperature, and heat transfer efficiency in dusty nanofluids [5,6]. This work explores the two-phase dusty fluid flow dynamics over a wavy surface [7]. They highlighted the enhancement of thermal properties through the use of hybrid nanofluids [8]. Additionally, the effects of non-uniform heat sources or sinks and induced magnetic fields on MHD flows across inclined surfaces have been studied [9,10]. Other significant studies have focused on thermal transfer in dusty fluids with variable properties over stretched sheets [11]. Research has also explored the effect of radiation on steady two-dimensional dusty fluid flows [12] and the dynamics of boundary layers and heat transfer in dusty fluid flows [13,14]. Inclined buoyancy forces in fluid flow result from the density variations due to temperature or concentration gradients, combined with gravity and inclination angle effects. Such forces influence flow behavior, stability, heat transfer, and boundary layer thickness, playing important roles in natural convection applications including cooling systems, solar collectors, and geophysical flows. Researchers analyzed the MHD boundary layer flow of a water-based nanofluid over a permeable inclined stretched sheet in a porous medium [15]. This study developed a framework to analyze the unstable MHD Powell-Eyring fluid flow over a slip-stretched surface, incorporating the effect of chemical reactions and nonlinear thermal radiation [16]. The researchers investigated the non-similar behavior of MHD hybrid nanofluid flow across a porous medium [17]. They numerically

investigated entropy generation in MHD Casson fluid flow over a wedge [18]. Scientists examined the effect of the stratification loss parameter on fluid momentum [19] and the time-dependent, incompressible flow of a two-dimensional thin-film nanofluid under nonlinear convection and magnetic effects [20]. Additionally, it has been studied how an angled magnetic field affects a Williamson nanofluid's mass, momentum, and heat transfer across a stretching sheet [21]. Figure 1(a) illustrates the application of inclined buoyancy forces with dust particles [22].

According to Darcy's law, a solid matrix makes up a medium that is porous with interconnected pores that permit fluid flow. Examples include rocks, dirt, and foams, which are used in heat transfer, groundwater flow, and filtration. They

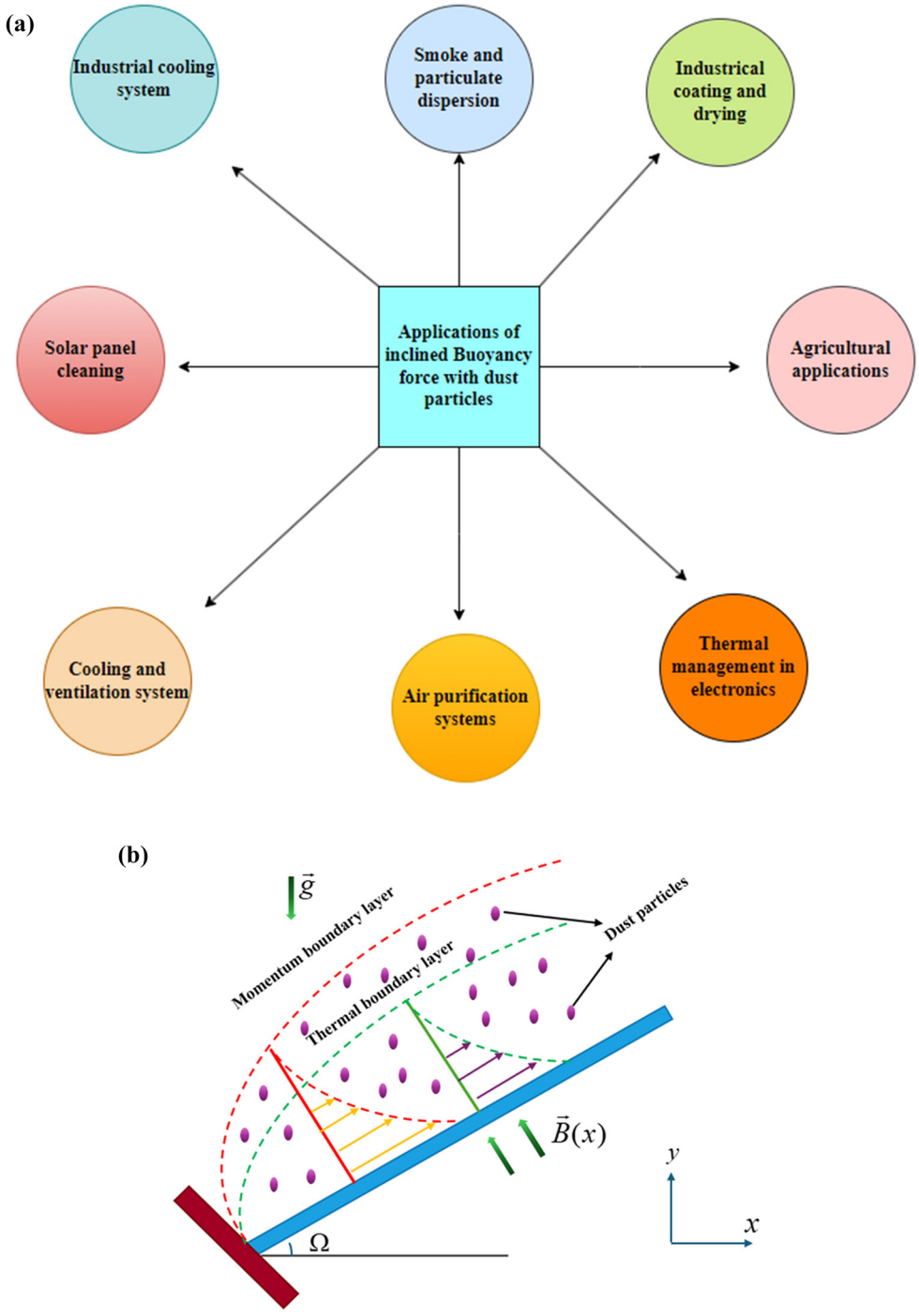

Figure 1: (a) Applications of inclined Buoyance force with dust particles. (b). Flow diagram.

investigated the MHD dusty fluid's peristaltic flow through a permeable layer, considering the consequence of temperature variance, heat source, and wall properties [23]. They studied the fluid flow and heat transfer characteristics of a hybrid nanofluid over stretching disks [24]. This theoretical analysis explored the dust particle velocity, fluid velocity, and skin-friction of dusty viscous fluid in a porous material while affected by a transverse magnetic field [25,26]. Using boundary layer approximations and Darcy's law, this study investigated the impact of slip on the MHD flow of a dusty fluid through a porous stretched sheet [27,28].

Response surface methodology (RSM) constitutes the statistical methodology utilized for the optimization of processes where the interrelations among multiple input variables and one or more response variables necessitate examination [29]. This methodology proves advantageous in identifying the optimal conditions under which a process can attain peak efficiency, quality, or yield, as it encompasses various experimental designs grounded in structured knowledge and regression analysis that aim to ascertain the most favorable operational parameters. This technique is of paramount importance in the domains of engineering, manufacturing, and product design [30].

Consequently, RSM minimizes the requisite number of experiments, thus conserving both time and resources, while simultaneously serving as a critical instrument in enhancing product quality, process efficiency, innovation, and sustainable development [31]. Researchers investigated unsteady flows aligned with the axis of a micropolar fluid within an annular domain featuring a porous layer [32]. The study encompassed an analytical exploration of a three-layered composite channel that was inclined and incorporated Hall current and cobalt ferrite nanoparticles within a Darcy medium [33].

In the current study, the heat transfer rate of nano and dusty fluids is considered under the inclined buoyancy force with a magnetic field effect. This effect is examined in the current study by using the numerical method bvp4c and RSM. The following are the novelties and significance added to the present work:

- The novelty of the research is to scrutinize the optimization and numerical study of nanofluid flow with dust particles,
- The analysis is also done for the local Grashof number and fluid interaction parameter for temperature,
- Analyze the skin friction and Nusselt number behavior,
- The numerical computation of the modeled problem is computed using bvp4c tool of MATLAB along with the implementation of shooting the algorithm,
- Additionally, RSM is used for the determination of statistical optimization.

2 Mathematical model

This study considers the steady, two-dimensional, laminar boundary layer flow of an incompressible, viscous, dusty nanofluid past across a vertically inclined stretching sheet. The sheet is positioned in the xy-plane, with the flow occurring in the upper region and aligned with x-axis. The y-axis remains perpendicular to the sheet. The stretching motion is induced by two equal and opposing forces acting along x-axis, generating velocity $u_x(x)$. A uniform magnetic field B_0 is applied along the x-axis, interacting with the conducting nanofluid, as depicted in Figure 1(b). Initially, both the fluid and the dust particles are considered at rest. The dust particles are assumed to be uniform in size, spherical in shape, and distributed with a constant number density throughout the flow. The model accounts for the drag force exerted between the fluid and dust particles. Additionally, the formulation includes the volume fraction of both nanoparticles and dust particles, ensuring a comprehensive representation of their interactive effects on heat and momentum transfer. The thermal energy exchange between the dust particles and the nanofluid is incorporated *via* specific energy equations.

Under these assumptions and employing the Boussinesq's approximation, the governing equations are formulated as described in earlier studies [34,35].

$$\frac{\partial u}{\partial x} + \frac{\partial v}{\partial y} = 0, \tag{1}$$

$$(1-\phi_{\mathrm{p}})\left(u\frac{\partial u}{\partial x} + v\frac{\partial u}{\partial y}\right) = (1-\phi_{\mathrm{p}})\nu_{\mathrm{nf}}\frac{\partial^2 u}{\partial x^2} + \frac{\mathrm{KN}}{\rho_{\mathrm{nf}}}(u_{\mathrm{p}}-u) - \frac{\nu_{\mathrm{nf}}}{k_1}u - \frac{\sigma B_0^2}{\rho_{\mathrm{nf}}}u + g\beta^*(T-T_\infty)\cos\alpha, \tag{2}$$

$$\frac{\partial u_p}{\partial x} + \frac{\partial v_{\mathrm{p}}}{\partial y} = 0, \tag{3}$$

$$u_{\mathrm{p}}\frac{\partial u_{\mathrm{p}}}{\partial x} + v_{\mathrm{p}}\frac{\partial u_{\mathrm{p}}}{\partial y} = \frac{K}{m}(u-u_{\mathrm{p}}), \tag{4}$$

$$(\rho c_{\mathrm{p}})_{\mathrm{nf}}\left(u\frac{\partial T}{\partial x} + v\frac{\partial T}{\partial y}\right) = k_{\mathrm{nf}}\frac{\partial^2 T}{\partial y^2} + \frac{N_1(c_{\mathrm{p}})_{\mathrm{nf}}}{\tau_{\mathrm{T}}}(T_{\mathrm{p}}-T) + \frac{N_1}{\tau_v}(u_{\mathrm{p}}-u)^2, \tag{5}$$

$$N_1 c_{\mathrm{m}}\left(u_{\mathrm{p}}\frac{\partial T_{\mathrm{p}}}{\partial x} + v_{\mathrm{p}}\frac{\partial T_{\mathrm{p}}}{\partial y}\right) = -\frac{N_1(c_{\mathrm{p}})_{\mathrm{nf}}}{\tau_{\mathrm{T}}}(T_{\mathrm{p}}-T). \tag{6}$$

With boundary conditions

$$u = u_w(x),\quad v = 0,\quad T = T_w = T_\infty + A(x/l)^2 \text{ at } y = 0, \tag{7}$$

$$u \to 0,\quad u_{\mathrm{p}} \to 0,\quad v_{\mathrm{p}} \to v,\quad T \to T_\infty,\quad T_{\mathrm{p}} \to T_\infty,\quad \text{as } y \to \infty. \tag{8}$$

We present the following similarity transformation for the similarity solution.

$$\begin{cases} u = cxf'(\zeta), \quad v = -v^{1/2}c^{1/2}f(\zeta), \quad \zeta = v^{-1/2}c^{1/2}y, \\ u_{\mathrm{p}} = cxF'(\zeta), \quad v_{\mathrm{p}} = -v^{1/2}c^{1/2}F(\zeta), \quad \theta(\zeta) = \dfrac{T - T_\infty}{T_w - T_\infty}, \\ \theta_{\mathrm{p}}(\zeta) = \dfrac{T_{\mathrm{p}} - T_\infty}{T_w - T_\infty}, \end{cases} \tag{9}$$

where

$$T - T_\infty = A(x/l)^2\theta(\zeta), \quad A > 0.$$

Transformed governing equations are

$$f''' - f'^2 + ff'' + \frac{\alpha\beta}{(1-\phi_{\mathrm{p}})}(F' - f') - \frac{(M + K_1)}{(1-\phi_{\mathrm{p}})}f' + \mathrm{Gr}\theta\cos\psi = 0, \tag{10}$$

$$F'^2 - FF'' + \beta(F' - f') = 0, \tag{11}$$

$$\theta'' - \mathrm{Pr}(2f'\theta - f\theta') + \mathrm{Pr}\alpha\beta_{\mathrm{T}}(\theta_{\mathrm{p}} - \theta) + \mathrm{Pr}\ \mathrm{Ec}\alpha(F'f')^2 = 0, \tag{12}$$

$$2F'\theta_{\mathrm{p}} - F\theta_{\mathrm{p}}' + \gamma\beta_T(\theta_{\mathrm{p}} - \theta) = 0. \tag{13}$$

The transformed boundary conditions are

$$\begin{cases} f'(\zeta) = 1, \quad f(\zeta) = 0 \ \text{ at } \ \zeta = 0 \\ f'(\zeta) = 0, \quad F'(\zeta) = 0, \quad F(\zeta) = f(\zeta) \ \text{ at } \ \zeta \to \infty, \end{cases} \tag{14}$$

$$\begin{cases} \theta(\zeta) = -\mathrm{Bi} * (1 - \theta(\zeta)) \ \text{ at } \ \zeta = 0 \\ \theta(\zeta) = 0, \quad \theta_{\mathrm{p}}(\zeta) = 0 \ \text{ at } \ \zeta \to \infty. \end{cases} \tag{15}$$

Here $\alpha = \frac{\mathrm{Nm}}{\rho_{\mathrm{nf}}}$ is the mass concentration of the dust particles, $M = \frac{\sigma B_0^2}{c\rho_{\mathrm{nf}}}$ is the magnetic field, $\beta = \frac{K}{c_{\mathrm{m}}}$ is the fluid particle interaction parameter for the velocity, $K_1 = \frac{v_{\mathrm{nf}}}{ck_1}$ is the porosity parameter, $\mathrm{Gr} = \frac{g\beta^*(T_w - T_\infty)}{cU_w}$ is the local Grashof number, $\mathrm{Pr} = \frac{\mu_{\mathrm{nf}}(c_{\mathrm{p}})_{\mathrm{nf}}}{k_{\mathrm{nf}}}$ is the Prandtl number, $\beta_{\mathrm{T}} = \frac{1}{c\tau_{\mathrm{T}}}$ is the fluid interaction parameter for temperature, $\mathrm{Ec} = \frac{cl^2}{A(c_{\mathrm{p}})_{\mathrm{nf}}}$ is the Eckert number, $\gamma = \frac{(c_{\mathrm{p}})_{\mathrm{nf}}}{\mathrm{cm}}$ is the specific heat of the nano fluid to dust particles, and $\mathrm{Bi} = \frac{h(v/a)^{1/2}}{k}$ is the Biot number.

The physical quantity of interest is the skin friction coefficient Cf, and local Nusselt number Nu_x that are defined as

$$\mathrm{Cf}\,\mathrm{Re}_x^{1/2} = f''(0), \quad \mathrm{Nu}_x\,\mathrm{Re}_x^{1/2} = -\theta'(0),$$

where $\mathrm{Re}_x^{1/2} = \frac{u_w(x)}{v_{\mathrm{nf}}}$ is the local Reynolds number.

2.1 Numerical scheme

In our study, we employed bvp4c, a boundary value problem (BVP) solver in MATLAB that uses fourth-order collocation based on a Lobatto quadrature formula. This finite-difference-based collocation method ensures high accuracy and stability in solving BVPs. It is particularly well-suited for handling the nonlinear differential equations governing the flow and heat transfer of nano and dusty fluids. For clarity, we have explicitly mentioned that bvp4c is a fourth-order numerical method in the manuscript.

To reduce the system of higher-order nonlinear ordinary differential equations (10)–(15) into a set of first-order differential equations, we introduce the following new variables:

$$B(1) = f, \quad B(2) = f', \quad B(3) = f'', \quad B(4) = F,$$
$$B(5) = F', \quad B(6) = \theta, \quad B(7) = \theta', \quad B(8) = \theta_{\mathrm{p}}.$$

Using the newly introduced variables, the system of equations (10)–(15) is rewritten as

$$f' = B(2)$$

$$f'' = B(3)$$

$$f''' = f'^2 - ff'' - \frac{\alpha\beta}{(1-\phi_{\mathrm{p}})}(F' - f') + \frac{(M + K_1)}{(1-\phi_{\mathrm{p}})}f' - \mathrm{Gr}\ \theta\cos\psi,$$

$$F' = B(5),$$

$$F'' = F'^2 + \beta(F' - f')/F,$$

$$\theta = B(7),$$

$$\theta' = \mathrm{Pr}(2f'\theta - f\theta') - \mathrm{Pr}\ \alpha\beta_{\mathrm{T}}(\theta_{\mathrm{p}} - \theta) - \mathrm{Pr}\ \mathrm{Ec}\alpha(F'f')^2,$$

$$\theta_{\mathrm{p}}' = 2F'\theta_{\mathrm{p}} + \gamma\beta_{\mathrm{T}}(\theta_{\mathrm{p}} - \theta)/F.$$

The boundary conditions for the system are set as

$$\text{At wall } \zeta = 0: \quad B(1) = 1, \quad B(2) = 0, \quad B(4) = 0, \quad B(6) = -\mathrm{Bi}(1 - B(6)),$$

$$\text{Away from the wall } \zeta \to \infty: \quad B(2) = 0, \quad B(4) = 0, \quad B(4) = B(1), \quad B(6) = 0, \quad B(8) = 0.$$

3 Results and discussion

The system of transformed equations (10)–(13) with conditions (14) and (15) has been analyzed numerically utilizing the built-in MATLAB function known as the bvp4c solver. Throughout the calculation $\alpha = 0.1$, $\beta = 3$, $\phi_{\mathrm{p}} = 0.1$, $M = 0.5$, $K_1 = 2$, $\mathrm{Pr} = 5$, $\beta_{\mathrm{T}} = 5$, $\gamma = 2$, $\mathrm{Ec} = 1.5$, $\mathrm{Gr} = 0.3$ and inclination angel

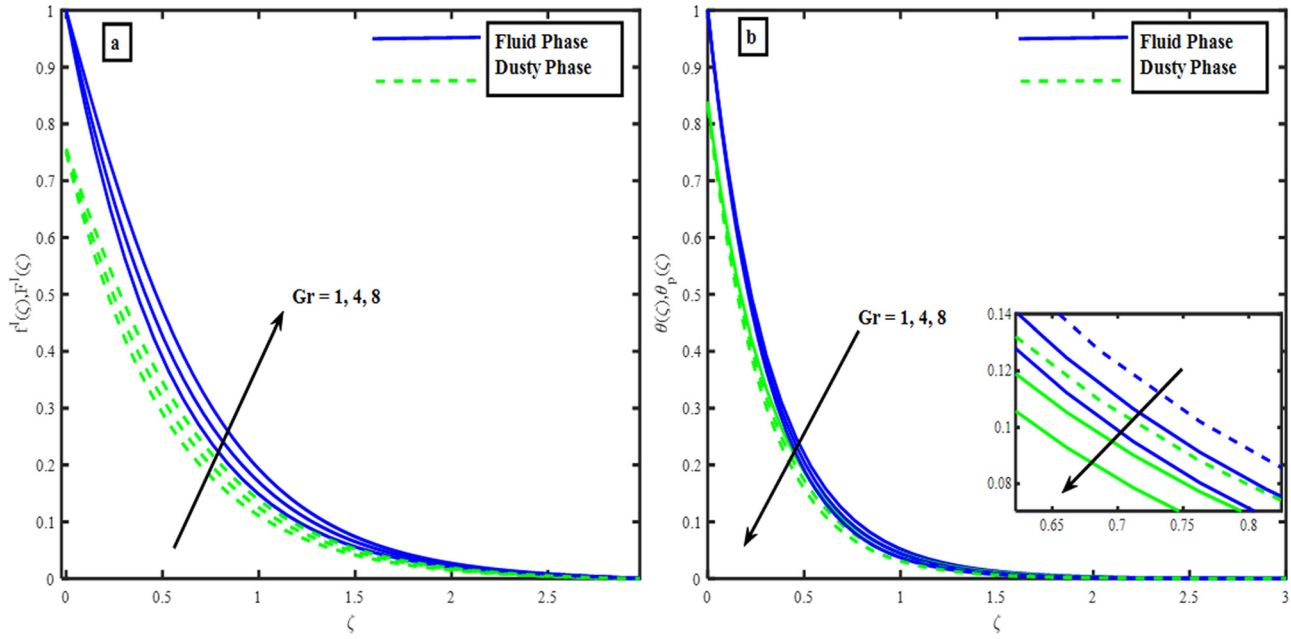

Figure 2: (a) Impact of Gr on velocity profile. (b) Impact of Gr on temperature profile.

$\Omega = \pi/3$, keeping constant across all analysis, except for variations illustrated in tables. In the graphical depictions, solid lines stand for the fluid phase while dashed lines denoted dusty phases. Figures 2–10 show the impact of various factors on temperature and velocity profiles.

Figure 2(a) and (b) indicates the gradients of velocity and temperature within the nanofluid and dust phases for diverse values of Gr. Clearly, a boost in the values of Gr causes the velocity to increase while concurrently inducing a decline in temperature. According to a physical interpretation of this phenomenon, this outcome demonstrates that reducing of the temperature boundary layer. The temperature and velocity gradients inside the nanofluid and dust phases for a range of M values are demonstrated in Figure 3(a) and (b). An increment in the values of M indicates the velocity to drop, concurrently enhancing the temperature.

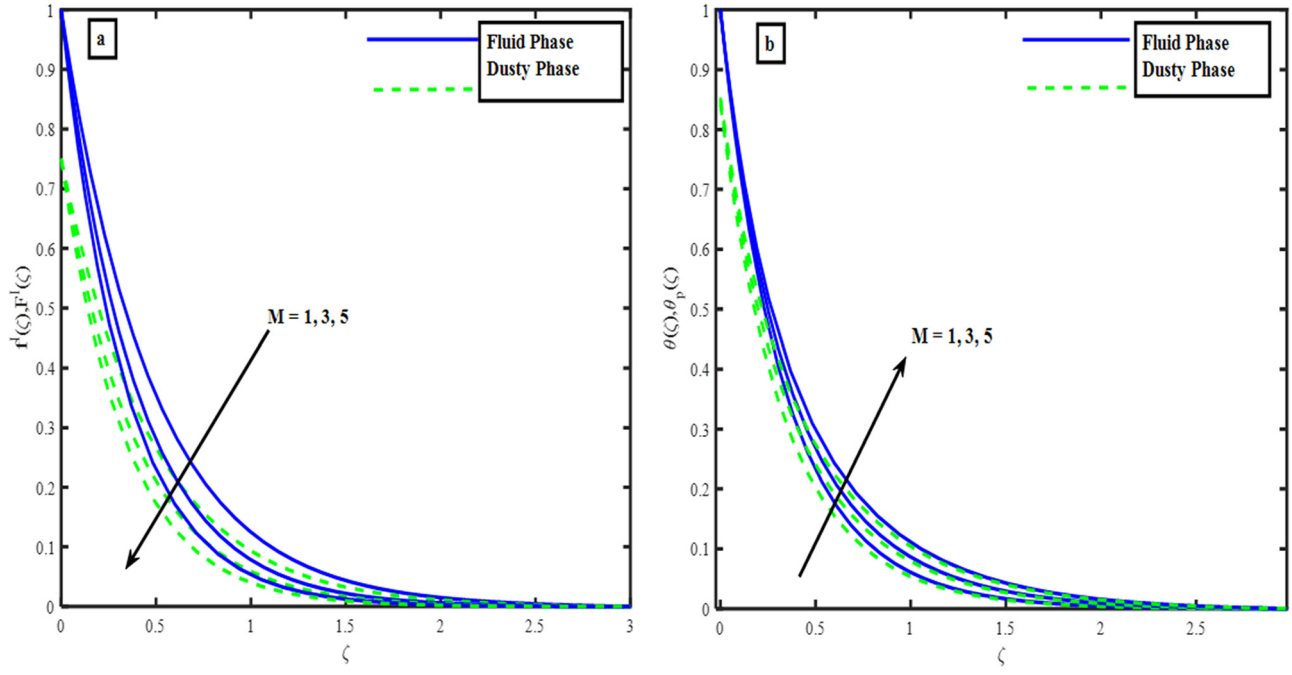

Figure 3: (a) Impact of M on velocity profile. (b) Impact of M on temperature profile.

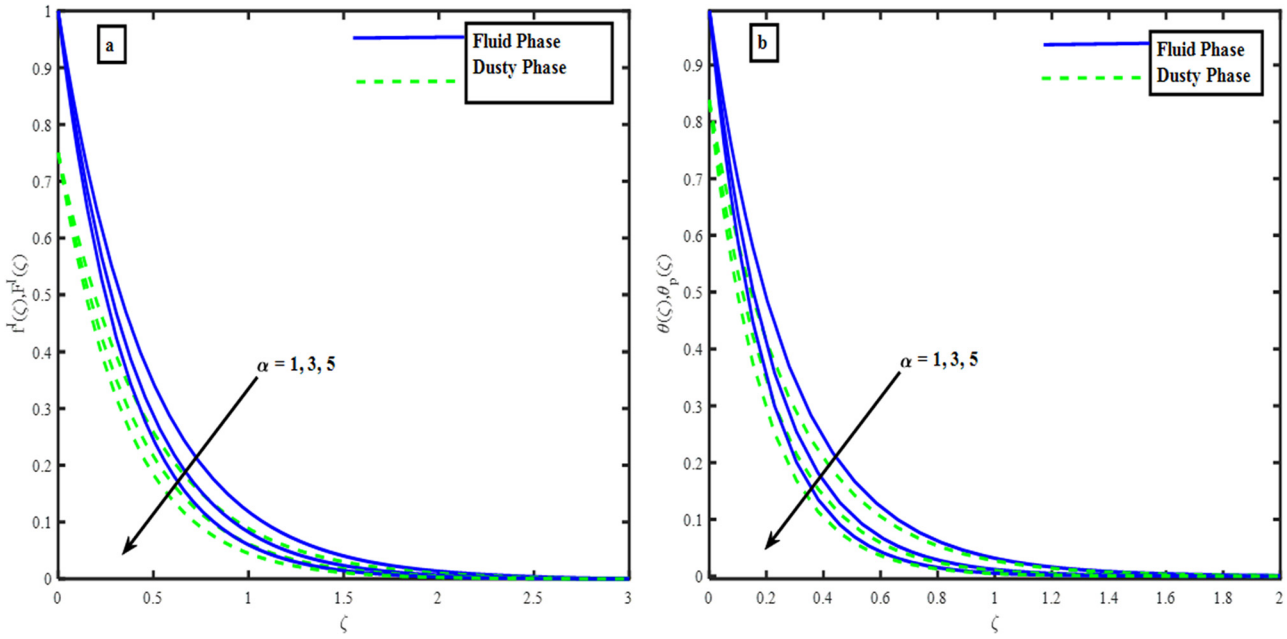

Figure 4: (a) Impact of α on velocity profile. (b) Impact of α on temperature profile.

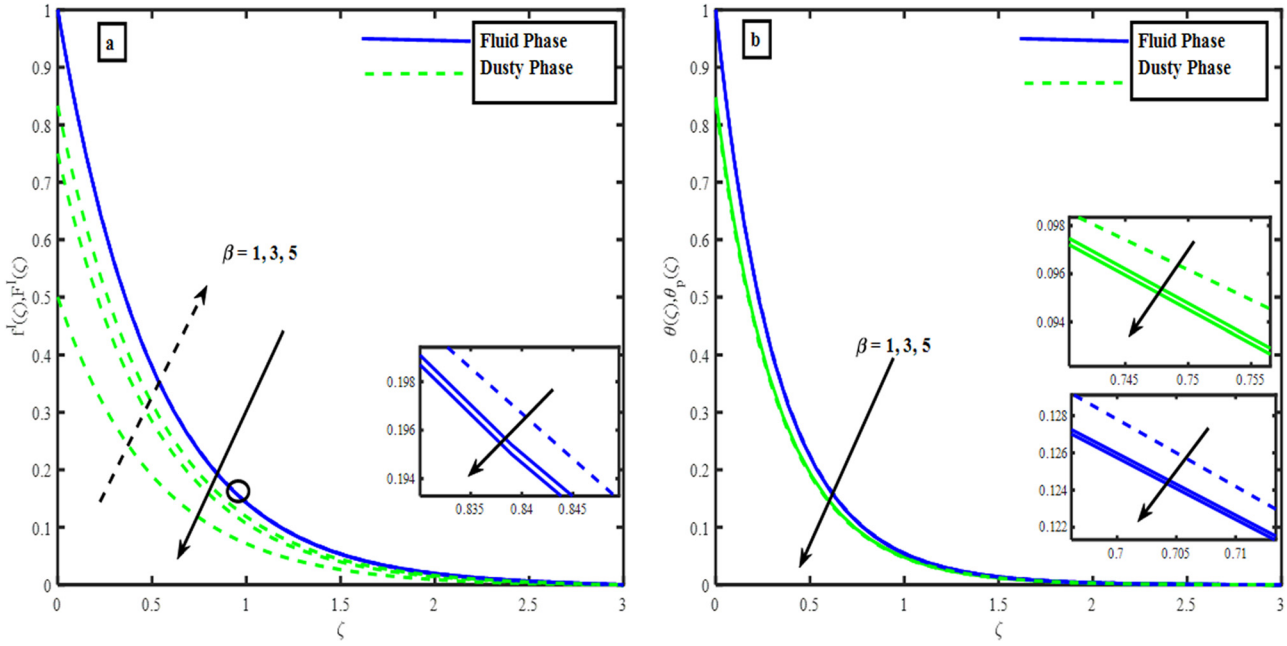

Figure 5: (a) Impact of β on velocity profile. (b) Impact of β on temperature profile.

Physically, the Lorentz forces are boosted with increases in magnetic parameter values, which cause the reduction in flow. Figure 4(a) and (b) illustrates the velocity gradient and temperature within the nanofluid and dusty fluid for various values of α. An increase in the values of α cause a decline in temperature and velocity profile. Physical interpretations of this phenomenon indicate that an increases in the mass concentration of dust particles is evident of a drop in the temperature and velocity boundary layers.

Figure 5(a) and (b) portray the fluctuations in the temperature and velocity profiles of the dust and nanofluid phases in response to alterations in β. From Figure 5(a), with the increment in the value of β, dust particle velocity increases while, nanofluid velocity decreases. This

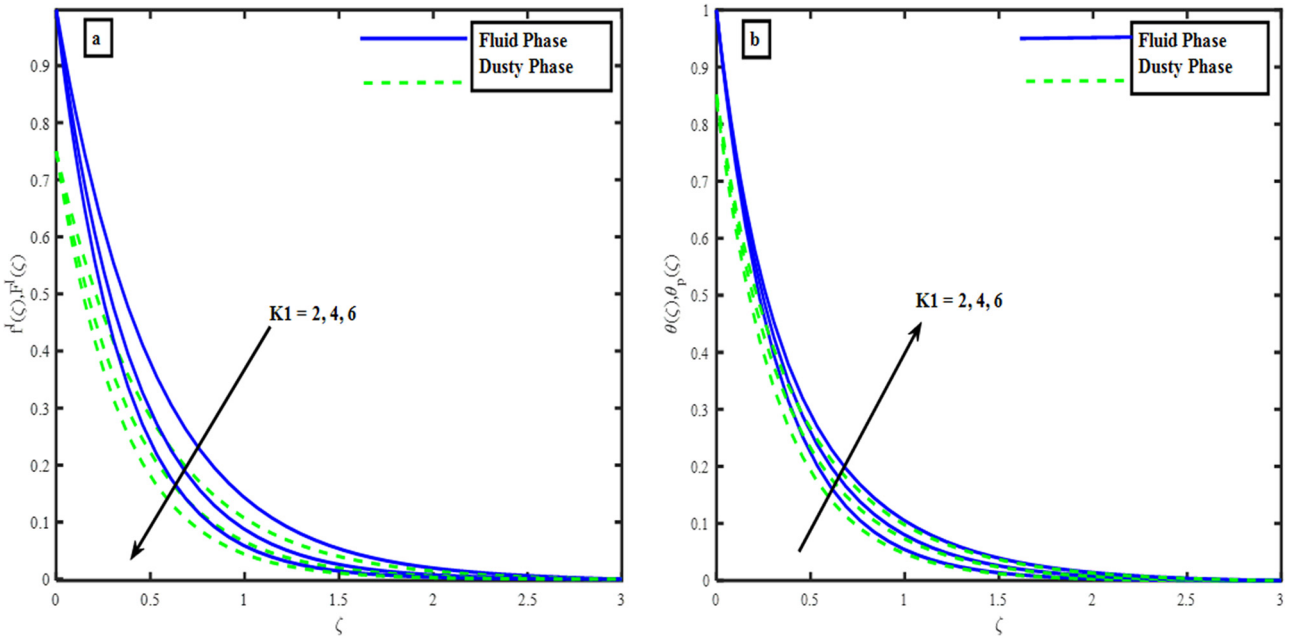

Figure 6: (a) Impact of K_1 on velocity profile. (b) Impact of K_1 on temperature profile.

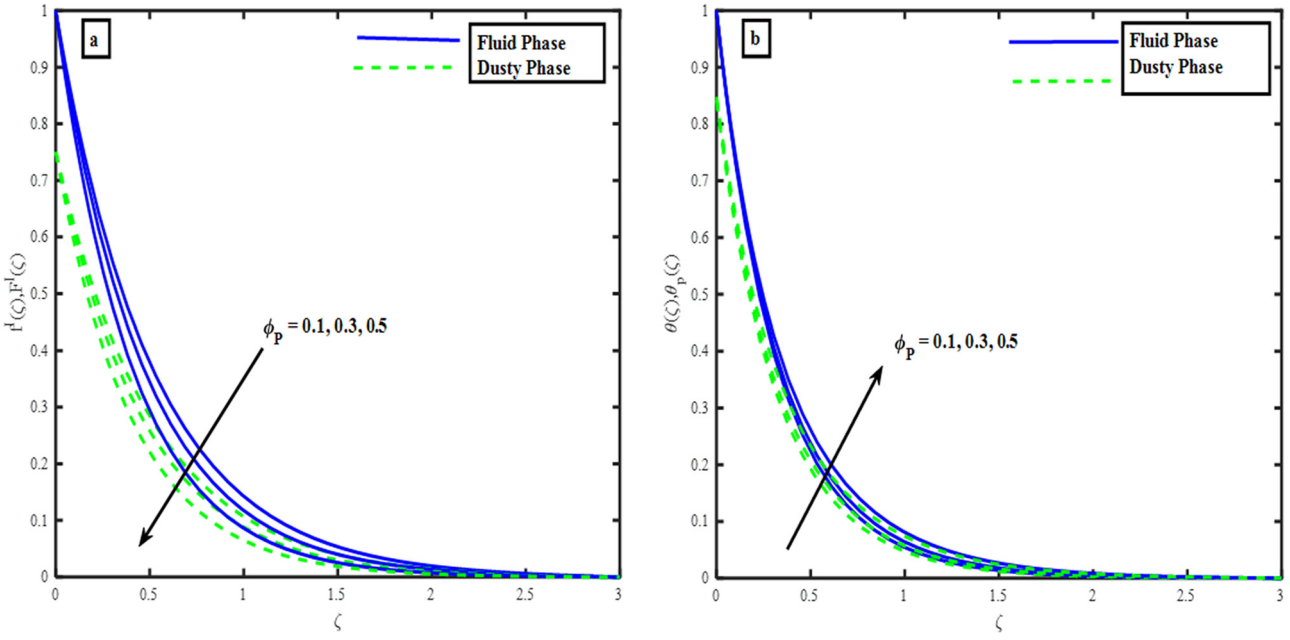

Figure 7: (a) Impact of ϕ_p on velocity and profile. (b) Impact of ϕ_p on temperature profile.

phenomenon occurs due to the stronger interaction between the particle phases and fluid. This occurs when the fluid phase is opposed by the particle phase until the particle velocity equals the fluids. Figure 5(b) indicates that as β increases, the temperature profile exhibits an upward trend. Physically, increased drag forces lead to greater energy dissipation, leaving less energy available for heat retention, which collectively lowers the temperature. Figure 6(a) and (b) delineates the effect of the parameter K_1 on both velocity and temperature in both dust phases and the nanofluid. Higher values of K_1 are associated with a decline in velocity and a rise in temperature across both phases. This occurs because an increment in the porosity parameter corresponds to larger pores in the porous

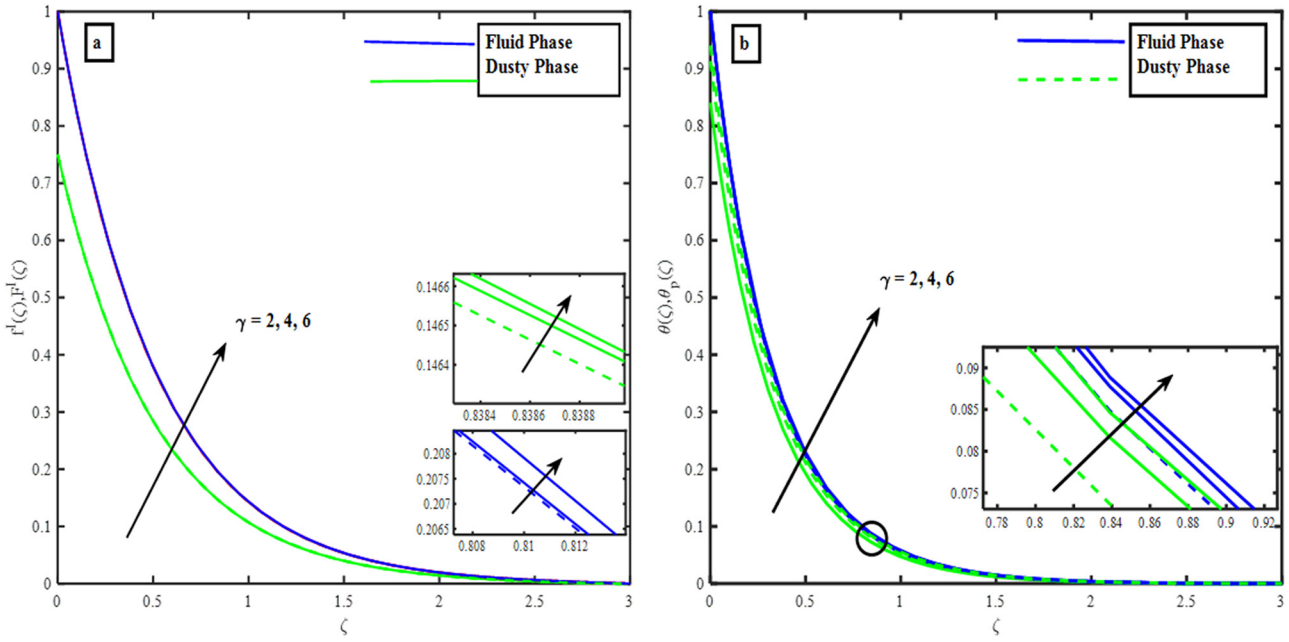

Figure 8: (a) Impact of γ on velocity and profile. (b) Impact of γ on temperature profile.

medium. As a result, resistive forces oppose the flow, diminishing the velocity profiles. Additionally, the increase in porosity facilitates the release of internal heat into the flow, leading to elevated temperature profiles in both the fluid and dust phases.

Figure 7(a) and (b) depicts the effect of dust particle volume fraction (ϕ_p) on temperature and velocity gradients. An increment in ϕ_p results in a reduced velocity profile and an increased temperature gradient. This behavior is attributed to the higher concentration of dust particles in the mixture, which increases the fluid density and reduces the width of the velocity boundary layer. Additionally, the higher dust particle content enhances the mixture's thermal conductivity, leading to elevated temperature profiles. The impact on the temperature and velocity profiles for the nanofluid and dust phases is depicted in Figure 8(a) and (b). The velocity profile drops, and the temperature gradient grows as γ increases. This trend is likely due to the higher specific heat capacity ratio between the nanoparticles and dust particles, allowing the mixture to absorb and retain more thermal energy.

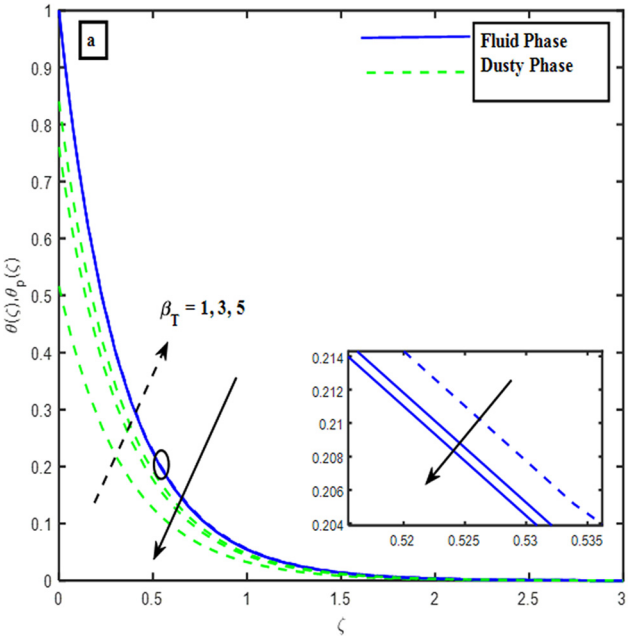

Figure 9: Impact of β_T on temperature profile.

Figure 9(a) demonstrates the effects of the interaction parameter for temperature β_T on the temperature profiles. Figure 9(a) shows that as β_T increases, the nanofluid temperature decreases while the dusty fluid temperature improves. This behavior may result from the improved interaction among the nanoparticle and dust particle phases, where conductive heat transfer is more prominent in the dust phase.

Figure 10 illustrates the comparison between Case 1 and Case 2 in terms of the Nusselt number across multiple runs. The figure provides a clear visualization of the differences in heat transfer characteristics between the two cases. Additionally, to further support the numerical data and enhance result interpretation. These additional figures offer a deeper and more detailed understanding of the results and validate the numerical findings effectively.

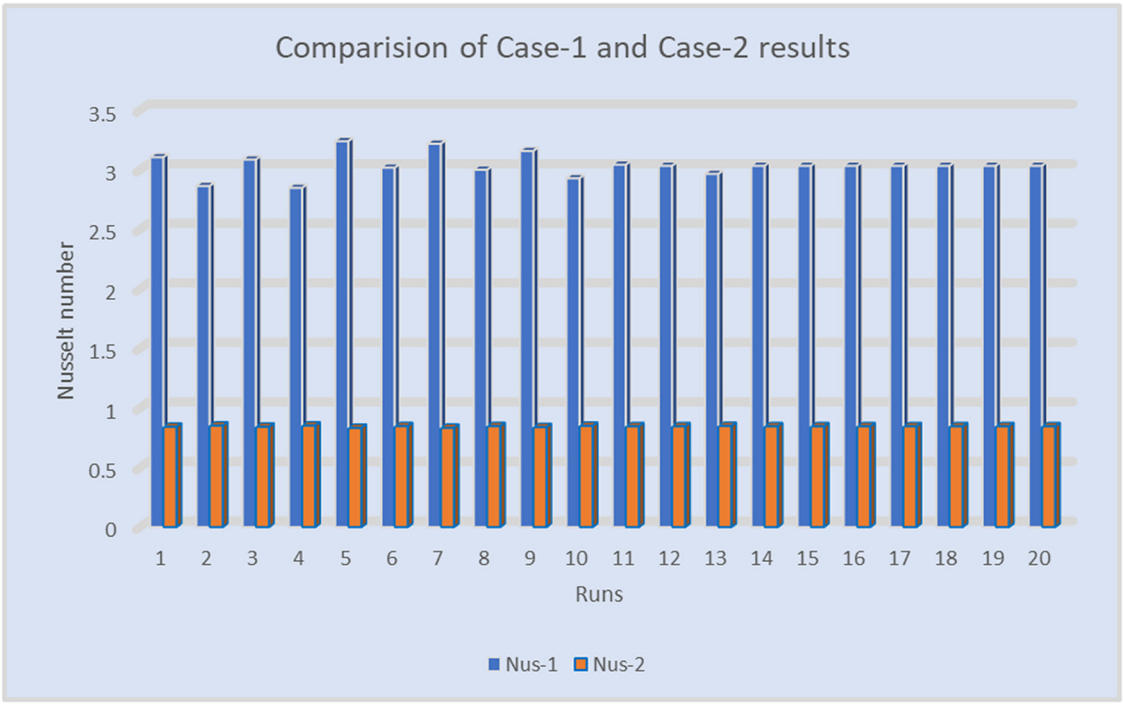

Figure 10: Comparison of Case 1 and Case 2 with Nusselt number.

3.1 RSM

RSM represents a comprehensive collection of statistical and mathematical methodologies utilized in the realm of experimental design, aimed at the enhancement of a system's response. The resultant output or response is typically contingent upon multiple independent variables. These input factors, commonly denoted as independent variables, frequently display interactive characteristics and may substantially affect the overall outcome, which is technically referred to as the "response." Within the paradigm of RSM, errors are perceived as stochastic phenomena, thereby augmenting the dependability of response predictions. This methodological approach is particularly beneficial in contexts where direct evaluations, such as finite element methods or computational fluid dynamics become excessively costly and temporally demanding; as a result, it alleviates the related expenses and computational complexities. RSM lessens the influence of extrinsic disturbances on outcomes by synchronizing the optimization process with the optimal conditions of

Table 1: RSM parameters, with their key factors, symbols, and levels

Key factors	Symbols	Levels		
		−1 (Low)	0 (Medium)	1 (High)
M	X_1	1	3	5
Ec	X_2	2	4	6
Gr	X_3	1	4	8

Table 2: Heat transfer rate experiment design and outcomes

Runs	Coded values			Real values			Response	
	X_1	X_2	X_3	M	Ec	Gr	Nus_1	Nus_2
1	−1	−1	−1	1	2	1	3.104788	0.842081
2	1	−1	−1	5	2	1	2.863469	0.852499
3	−1	1	−1	1	6	1	3.085273	0.842255
4	1	1	−1	5	6	1	2.847711	0.852602
5	−1	−1	1	1	2	8	3.239577	0.832719
6	1	−1	1	5	2	8	3.017428	0.84667
7	−1	1	1	1	6	8	3.21768	0.832878
8	1	1	1	5	6	8	2.999941	0.846787
9	−1	0	0	1	4	4	3.157547	0.838154
10	1	0	0	5	4	4	2.928464	0.850075
11	0	−1	0	3	2	4	3.042509	0.845496
12	0	0	0	3	4	4	3.033439	0.845564
13	0	0	−1	3	4	1	2.965272	0.848649
14	0	0	0	3	4	4	3.033439	0.845564
15	0	0	0	3	4	4	3.033439	0.845564
16	0	0	0	3	4	4	3.033439	0.845564
17	0	0	0	3	4	4	3.033439	0.845564
18	0	0	0	3	4	4	3.033439	0.845564
19	0	0	0	3	4	4	3.033439	0.845564
20	0	0	0	3	4	4	3.033439	0.845564

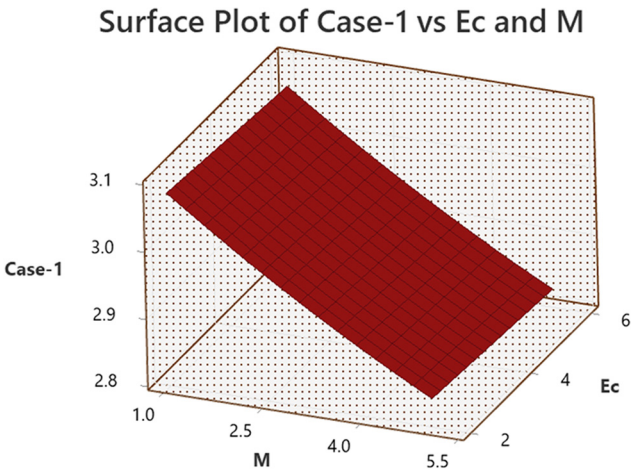

Figure 11: Surface plot of Nus_1 *vs* Ec and M.

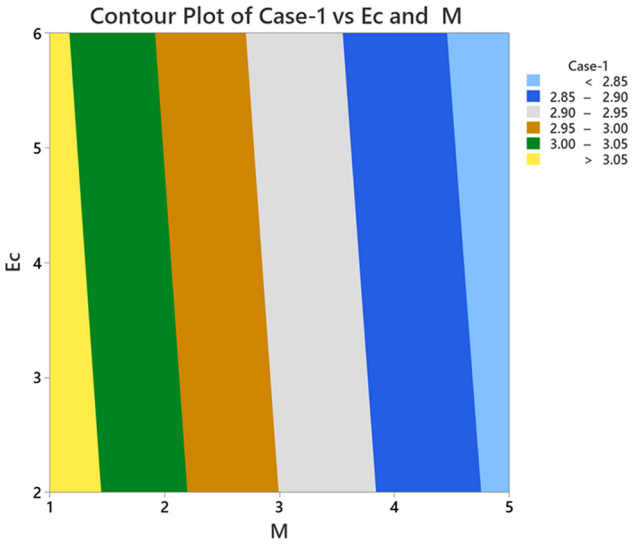

Figure 12: Contour plot of Nus_1 *vs* Ec and M.

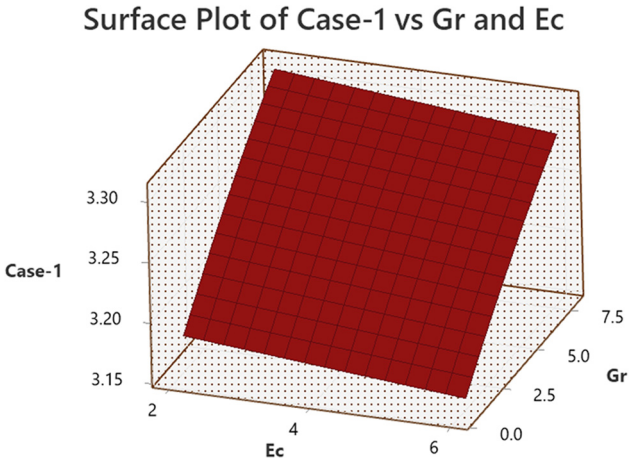

Figure 13: Surface plot of Nus_1 *vs* Gr and Ec.

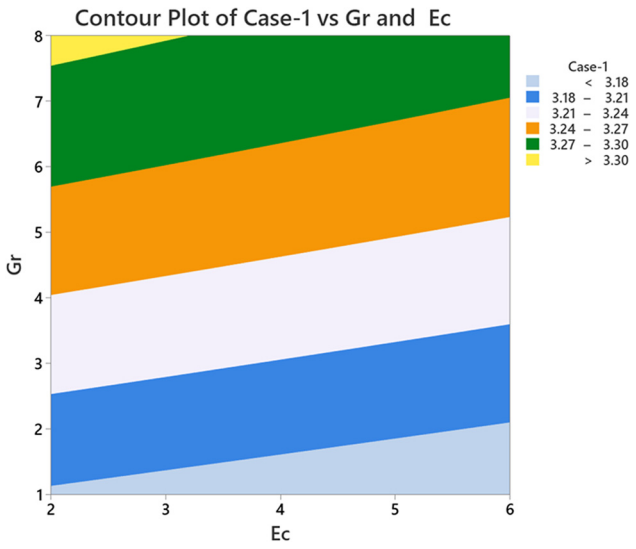

Figure 14: Contour plot of Nus_1 *vs* Gr and Ec.

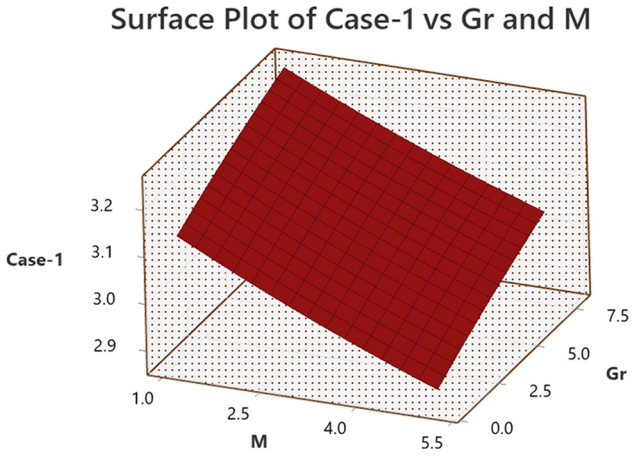

Figure 15: Surface plot of Nus_1 *vs* Gr and M.

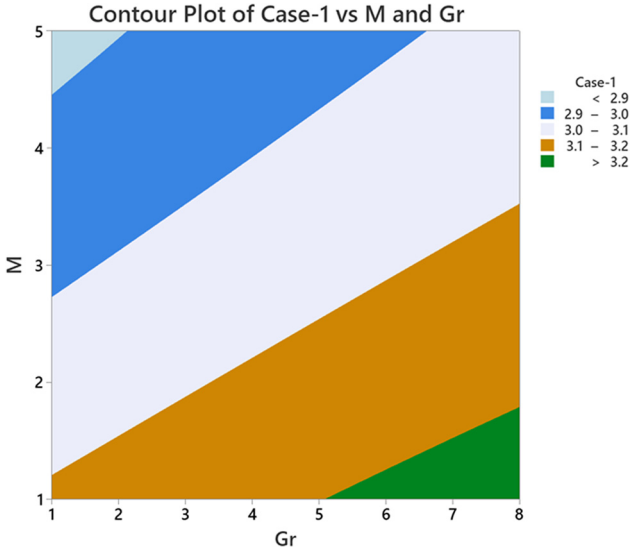

Figure 16: Contour plot of Nus_1 *vs* M and Gr.

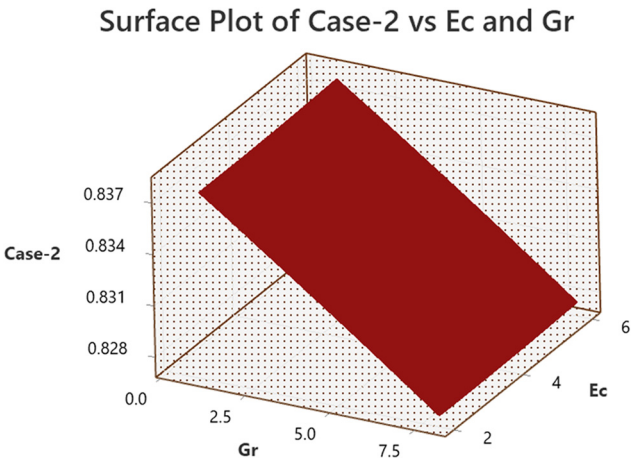

Figure 17: Surface plot of Nus_2 *vs* Ec and Gr.

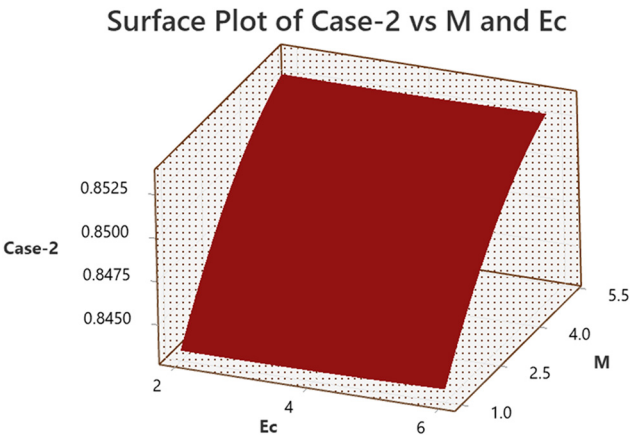

Figure 19: Surface plot of Nus_2 *vs* M and Ec.

the input variables. It encompasses various design types of RSM, including Box-Behnken, central composite design, and D-Optimal; each of these designs possesses unique advantages that facilitate the efficient investigation of factor interactions, thereby supporting the optimization process.

3.1.1 RSM optimization outcomes

This investigation is comprised of three principal components, magnetic field (M), Eckert number (Ec), and local Grashof number (Gr). These parameters are investigated to determine the optimal values for enhancing the rate of heat transfer. Each variable is assessed across three separate tiers, high (1), medium (0), and low (−1). The key variables, their respective levels, and the associated coded values are concisely presented in Table 1. According to the design outlined in Table 2, a total of 20 experimental trials are required, derived from the formula $F + 2N + 2^N$, where F denotes the number of factors and N signifies the number of levels applicable to each factor.

3.1.2 RSM graphical analysis

Figures 11–22 illustrate the variations in two-dimensional contour plots and three-dimensional surface plots related to various parameters for the Nusselt number of nanofluids (Nus_1) and dusty phases (Nus_2). Figures 11 and 12 focus on the relationship between the Eckert number (Ec) and magnetic field (M) concerning the Nusselt number (Nus_1). The three-dimensional surface plot visually represents how the Nusselt number fluctuates

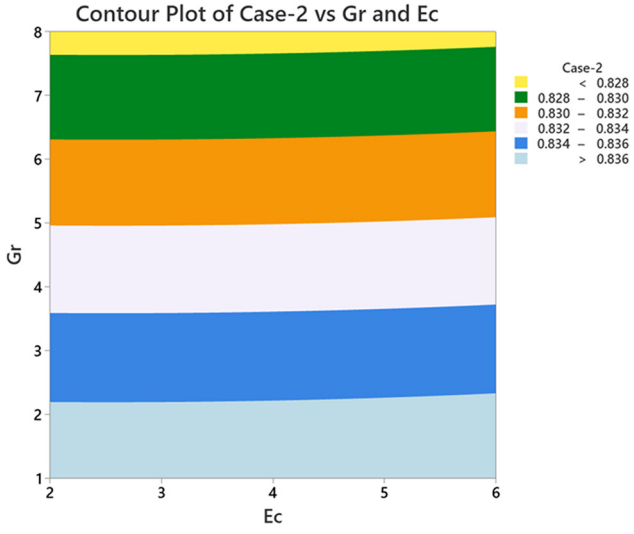

Figure 18: Contour plot of Nus_2 *vs* Gr and Ec.

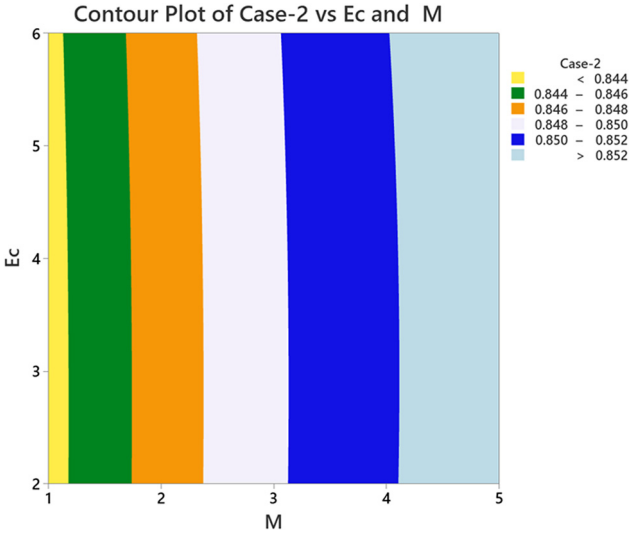

Figure 20: Contour plot of Nus_2 *vs* Ec and M.

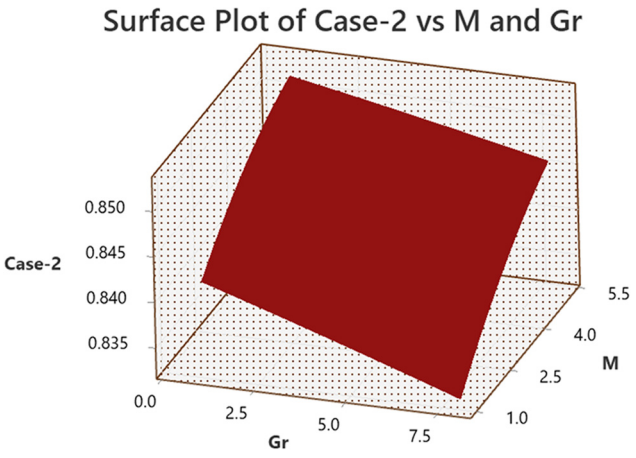

Figure 21: Surface plot of Nus_2 *vs* M and Gr.

under different conditions of both the Ec and M. It is clear that a development in the Eckert number correlates with a decline in the Nusselt number. The contour plot further illustrates that as both Ec and M increase, the rate of heat transfer also decreases. Figures 13 and 14 present the surface plot and contour plot of (Nus_1) concerning the (Gr) and (Ec). The surface plot indicates that the Nusselt number value is increasing with increases in both Gr and Ec, while the contour plot confirms that the heat transfer rate is positively influenced by increases in these parameters. Figures 15 and 16 illustrate the surface plot and contour plot for (Nus_1) in relation to the local Grashof number (Gr) and the magnetic field (M). From these plots, it is evident that the rate of thermal transfer is decreased with the increment in both M and Gr. Figures 17 and 18 depict the surface plot and contour plot for (Nus_2) (dusty fluid), showing that as both the local Grashof number and the Eckert number increases, the rate

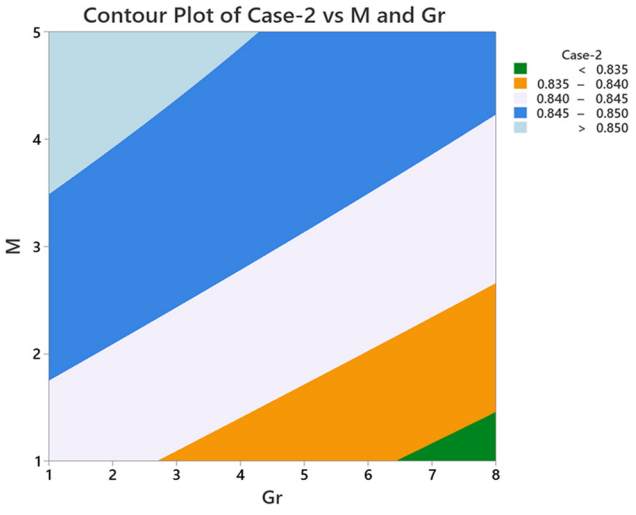

Figure 22: Contour plot of Nus_2 *vs* M and Gr.

Table 3: This table shows the skin friction and nusselt number for the fluid phase case

M	α	β	β_T	K_1	γ	Ec	ϕ_P	Gr	$-f''(0)$	$-\theta'(0)$
1.0									2.072139	3.090882
3.0									2.548240	2.958027
5.0									2.949437	2.845949
	1.0								2.121407	3.616987
	3.0								2.484541	4.527131
	5.0								2.800470	5.288498
		1.0							1.928040	3.105494
		3.0							1.935286	3.128804
		5.0							1.937677	3.133205
			1.0						1.935102	3.101575
			3.0						1.935242	3.122112
			5.0						1.935286	3.128804
				2.0					1.935286	3.128804
				4.0					2.437805	2.988922
				6.0					2.854360	2.872443
					2.0				1.935286	3.128804
					4.0				1.935054	3.095965
					6.0				1.934967	3.083702
						2.0			1.935272	3.126303
						4.0			1.935213	3.116297
						6.0			1.935154	3.106292
							0.1		1.935286	3.128804
							0.3		2.133678	3.073778
							0.5		2.451317	2.985143
								1.0	1.866490	3.144675
								4.0	1.580726	3.206252
								8.0	1.217371	3.276760

of heat transfer decline. Figures 19 and 20 analyze the surface and contour plots of (Nus_2) against the Magnetic field (M) and the Eckert number (Ec), revealing that the thermal transfer rate rises with greater values of M and Ec. Finally, the surface plots and contour plots of (Nus_2) in relation to the magnetic field (M) and the local Grashof number (Gr) are displayed in Figures 21 and 22. It is shown that a drop in the Nusselt number occurs when both Gr and M increase. Overall, the results from these figures underscore the significant influence of the local Grashof number, magnetic field, and Eckert number on the heat transfer rates in both nanofluids and dusty fluids.

Tables 3 and 4 display the fluctuations in skin friction and Nusselt number for the nanofluid phase and dust phase. The magnetic field (M), volume fraction of dust particles (ϕ_P), porosity parameter (K_1), and fluid interaction parameter for temperature (β_T) increases, skin friction for nanofluid and Nusselt number for dusty fluid increases while skin friction for dust particle and Nusselt number of nanofluid decreases. More viscous dissipation results from increasing Eckert number (Ec), which reduces skin friction and the Nusselt number in the fluid and dust phases and for the Ratio of specific heat of nano particles to

Table 4: This table represents the skin friction and nusselt number for the dusty phase case

M	α	β	β_{T}	K_1	γ	Ec	ϕ_{P}	Gr	$F'(0)$	$\theta_{\mathrm{p}}(0)$
1.0									0.750098	0.843008
3.0									0.749996	0.849284
5.0									0.749946	0.853057
	1.0								0.750129	0.838974
	3.0								0.750101	0.836746
	5.0								0.750082	0.835489
		1.0							0.500270	0.848173
		3.0							0.750144	0.840669
		5.0							0.833425	0.838265
			1.0						0.750142	0.516367
			3.0						0.750144	0.760420
			5.0						0.750144	0.840669
				2.0					0.750144	0.840669
				4.0					0.750013	0.848034
				6.0					0.749957	0.852259
					2.0				0.750144	0.840669
					4.0				0.750141	0.913477
					6.0				0.750136	0.940607
						2.0			0.750144	0.840693
						4.0			0.750144	0.840789
						6.0			0.750143	0.840884
							0.1		0.750144	0.840669
							0.3		0.750081	0.843969
							0.5		0.750011	0.848194
								1.0	0.750475	0.839640
								4.0	0.752507	0.835302
								8.0	0.756392	0.829558

Table 5: Comparison of the results for temperature gradient $-\theta'(0)$

M	Abel and Mahesha [35]	Naramgari and Sulochana [33]	Present study
1	1.132413	1.132423	1.132420
2	1.062415	1.062415	1.062419
3	1.008080	1.008081	1.008079

dust particles (γ) parameter raises means in both the cases skin friction and nusselt number decreasing, but opposite behavior is observed in fluid particle interaction parameter for velocity (β). Skin friction and the nusselt number both rise with the mass concentration of dust particles (α) in the fluid phase, but the tendency reverses in the dusty phase. However, with an increment in the Gr values, skin friction in dusty phase and Nusselt number in nanofluid exhibits an increasing effect, while heat transfer rate increases in dusty fluid and skin friction value in nanofluid shows a decreasing effect.

To validate the present numerical model, Table 5 presents a comparative analysis with data from previously published research. The results exhibit a strong agreement between the values, demonstrating the reliability of the current approach.

4 Conclusion

In this study, the RSM has been applied to optimize the velocity and heat transfer of nanofluid including dust particles through inclined stretching sheet. The influence of the flow problem has been considered in terms of velocity and thermal effect. According to the computational results, nanofluid containing dust particles are extremely important and has many uses in automotive engines, heat exchangers, chillers, and other technical domains. The most important results are summarized as follows.

- Velocity gradient of nanofluid and dust particles phase increases with the increment in the local Grashof number, while the temperature profile shows decreasing behavior,
- On the other hand, behavior of temperature and velocity profile is opposite for magnetic field and porosity parameter,
- With the rising values of dust particle volume fraction, there is a tendency for it to decelerate the velocity and increases the flow's temperature profiles,
- It is noted that for a dusty fluid, the Nusselt number increases with the increases in M, α, β, β_T, K_1, γ, ϕ_{p}, and Ec, while for other parameters, it decreases. For nanofluid, this is increased by increasing Gr and Pr,
- The skin friction values for the dusty fluid are increased with M, α, β, β_{T}, K_1, and ϕ_{p}, while k_1 shows a decline.

Additionally, the study highlights the significant role of dusty fluid interactions in controlling thermal transport properties under MHD and porous media influence. These results offer a foundation for optimizing thermal management systems and suggest avenues for future research on hybrid nanofluids, unsteady flows, and fractional modeling techniques.

Acknowledgments: The authors acknowledge the support by the Korea Institute of Energy Technology Evaluation and Planning (KETEP) and the Ministry of Trade, Industry & Energy (MOTIE) of the Republic of Korea (No. RS-2025-02315209).

Funding information: The support by the Korea Institute of Energy Technology Evaluation and Planning (KETEP) and the Ministry of Trade, Industry & Energy (MOTIE) of the Republic of Korea (No. RS-2025-02315209).

Author contributions: U.A.: data curation; software; and writing – original draft. M.D.K.: formal analysis; resources; and software. A.A.: supervision; validation; and writing – review and editing. N.A.S.: methodology; resources; and software. J.D.C.: formal analysis; validation; and writing – review and editing. All authors have accepted responsibility for the entire content of this manuscript and approved its submission.

Conflict of interest: The authors state no conflict of interest.

Data availability statement: All data generated or analyzed during this study are included in this published article.

References

[1] Cengel Y, Cimbala J. Fluid mechanics fundamentals and applications. New York, USA: Mc Graw Hill; 2013.

[2] Yamaguchi H. Engineering fluid mechanics. Berlin, Germany: Springer Science & Business Media; 2008.

[3] Saffman PG. On the stability of laminar flow of a dusty gas. J Fluid Mech. 1962;13:120–8. doi: 10.1017/S0022112062000555.

[4] Chakrabarti A, Gupta AS. Hydromagnetic flow and heat transfer over a stretching sheet. Q Appl Math. 1979;37(1):73–8.

[5] Hussain M, Ali B, Awan AU, Alharthi M, Alrashedi Y. Role of nanoparticle radius for heat transfer optimization in MHD dusty fluid across stretching sheet. J Therm Anal Calorim. 2024;149(24):15179–92. doi: 10.1007/s10973-024-13738-9.

[6] Singh AK, Singh NP. MHD flow of a dusty viscoelastic liquid through a porous medium between two inclined parallel plates. Proc Natl Acad Sci, India Sect A, Phys Sci. 1996;66(pt. 2):143–50.

[7] Siddiqa S, Abrar MN, Hossain MA, Awais M. Dynamics of two-phase dusty fluid flow along a wavy surface. Int J Nonlinear Sci Numer Simul. 2016;17(5):185–93. doi: 10.1515/ijnsns-2015-0044.

[8] Abrar MN, Kosar S, Razzaq R. Thermal investigation of micro-polar tangent hyperbolic flow using a hybrid nanofluid approach. J Appl Phys. 2024;137(3):34302. doi: 10.22541/au.171785383.38918385/v1.

[9] Johan NA, Mansur S. Boundary layer flow of dusty nanofluid over stretching sheet with partial slip effects. J Adv Res Fluid Mech Therm Sci. 2021;87(2):118–26.

[10] Konch J, Hazarika GC. Effects of variable viscosity and thermal conductivity on MHD free convection flow of dusty fluid along a vertical stretching sheet with heat generation. Int Res J Eng Technol. 2016;3(2):1029–38.

[11] Gireesha BJ, Ramesh GK, Lokesh HJ, Bagewadi CS. Boundary layer flow and heat transfer of a dusty fluid over a stretching vertical surface. Appl Math. 2011;2(4):475–81. doi: 10.4236/am.2011.24061.

[12] Ramesh GK, Gireesha BJ. Flow over a stretching sheet in a dusty fluid with radiation effect. J Heat Transf. 2013;135(10):102702. doi: 10.1115/1.4024587.

[13] Mishra SK, Rauta AK. Boundary layer flow & heat transfer of an unsteady dusty fuid over a stretching sheet. Int J Sci Eng Res. 2015;6:182–9.

[14] Roy NC, Saha G. Heat and mass transfer of dusty Casson fluid over a stretching sheet. Arab J Sci Eng. 2022;47(12):16091–101. doi: 10.1007/s13369-022-06854-x.

[15] Bansal S, Pal J, Bisht MS, Fartyal P. Influence of nanofluids on boundary layer flow over an inclined stretching sheet in a porous media along with magnetic field. Int J Math Eng Manag Sci. 2024;9(2):267–82. doi: 10.33889/IJMEMS.2024.9.2.014.

[16] Parmar A, Kumar P, Choudhary R, Garg S, Jain A. Unsteady inclined MHD Powell-Eyring fluid with microorganisms over an inclined permeable stretching sheet with zero mass flux and slip condition. Int J Appl Comput Math. 2024;10(5):148. doi: 10.1007/s40819-024-01780-y.

[17] Razzaq R, Abrar MN, Sagheer S, Farooq U. Non-similar investigation of magnetohydrodynamics hybrid nanofluid flow over a porous medium with Joule heating and radiative effects. Chaos Solitons Fractals. 2024;189:115700. doi: 10.1016/j.chaos.2024.115700.

[18] Abrar MN, Kosar S. Entropy generation and heat transfer characteristics in MHD Casson fluid flow over a wedge with viscous dissipation and thermal radiation. ZAMM-Journal Appl Math Mech/Z Angew Math Mech. 2024;e202300666. doi: 10.1002/zamm.202300666.

[19] Kalpana G, Saleem S. Heat transfer of magnetohydrodynamic stratified dusty fluid flow through an inclined irregular porous channel. Nanomaterials. 2022;12(19):3309. doi: 10.3390/nano12193309.

[20] Saeed A, Kumam P, Nasir S, Gul T, Kumam W. Non-linear convective flow of the thin film nanofluid over an inclined stretching surface. Sci Rep. 2021;11(1):18410. doi: 10.1038/s41598-021-97576-x.

[21] Srinivasulu T, Goud BS. Effect of inclined magnetic field on flow, heat and mass transfer of Williamson nanofluid over a stretching sheet. Case Stud Therm Eng. 2021;23:100819. doi: 10.1016/j.csite.2020.100819.

[22] Reddy MS, Raju GSS, Reddy MS, Jayalakshmi K. Peristaltic MHD flow of a Bingham fluid through a porous medium in a channel. Afr J Sci Res. 2011;3(1):179–203.

[23] Sharma DK, Kirti D. MHD flow of dusty viscous fluid through a porous medium bounded by an oscillating porous plate in slip flow regime. J Emerg Technol Innov Res. 2022;9:2349–5162.

[24] Zada J, Khan A, Farooq M, Alsubaie AS, Rezapour S, Inc M. Computation of stretching disks fluid flow of hybrid nanofluid under the effect of variable magnetic field. ZAMM-J Appl Math Mech/Z Angew Math Mech. 2025;105(1):e202400114. doi: 10.1002/zamm.202400114.

[25] Bhatti MM, Zeeshan A, Ijaz N, Bég OA, Kadir A. Mathematical modelling of nonlinear thermal radiation effects on EMHD peristaltic pumping of viscoelastic dusty fluid through a porous medium duct. Eng Sci Technol Int J. 2017;20(3):1129–39. doi: 10.1016/j.jestch.2016.11.003.

[26] Abbas Z, Hasnain J, Sajid M. Effects of slip on MHD flow of a dusty fluid over a stretching sheet through porous space. J Eng Thermo Phys. 2019;28:84–102. doi: 10.1134/S1810232819010077.

[27] Ezzat MA, El-Bary AA, Morsey MM. Space approach to the hydro-magnetic flow of a dusty fluid through a porous medium. Comput Math Appl. 2010;59(8):2868–79. doi: 10.1016/j.camwa.2010.02.004.

[28] Kumar MD, Ahammad NA, Raju CSK, Yook SJ, Shah NA, Tag SM. Response surface methodology optimisation of dynamical solutions of Lie group analysis for nonlinear radiated magnetised unsteady wedge: Machine learning approach (gradient descent). Alex Eng J. 2023;74:29–50. doi: 10.1016/j.aej.2023.05.009.

[29] Sajjan K, Shah NA, Ahammad NA, Raju CSK, Kumar MD, Weera W. Nonlinear Boussinesq and Rosseland approximations on 3D flow in an interruption of Ternary nanoparticles with various shapes of densities and conductivity properties. AIMS Math. 2022;7(10):18416–49. doi: 10.3934/math.20221014.

[30] Farooq U, Imran M, Fatima M. Computational insights into the thermal behavior of SWCNT-Fe_3O_4 and MWCNT-CuO hybrid nanofluids in stretching cylinder with response surface methodology. Multiscale and Multidiscip Model. Exp. and Des. 2025;8(4):221.

[31] Shah SZH, Ayub A, Sabir Z, Adel W, Shah NA, Yook SJ. Insight into the dynamics of time-dependent cross nanofluid on a melting surface subject to cubic autocatalysis. Case Stud Therm Eng. 2021;27:101227. doi: 10.1016/j.csite.2021.101227.

[32] Subray PA, Hanumagowda BN, Raju CSK, Varma SVK, Jagdish P, Yook SJ, et al. Analytical analysis of inclined three-layered composite channel with cobalt ferrite nanoparticles and Hall current in Darcy medium. Propuls Power Res. 2023;12(4):523–38. doi: 10.1016/j.jppr.2023.11.001.

[33] Naramgari S, Sulochana C. MHD flow of dusty nanofluid over a stretching surface with volume fraction of dust particles. Ain Shams Eng J. 2016;7(2):709–16. doi: 10.1016/j.asej.2015.05.015.

[34] Ramesh GK, Gireesha BJ, Bagewadi CS. Heat transfer in MHD dusty boundary layer flow over an inclined stretching sheet with non-uniform heat source/sink. Adv Math Phys. 2012;2012(1):657805. doi: 10.1155/2012/657805.

[35] Abel MS, Mahesha NJAMM. Heat transfer in MHD viscoelastic fluid flow over a stretching sheet with variable thermal conductivity, non-uniform heat source and radiation. Appl Math Model. 2008;32(10):1965–83. doi: 10.1016/j.apm.2007.06.038.